SPECTRAL OBSERVATIONS OF THE EXTREME ULTRAVIOLET BACKGROUND

SIMON E. LABOV[1] AND STUART BOWYER[2]

Center for Extreme Ultraviolet Astrophysics, University of California, Berkeley, CA 94720

ABSTRACT

A grazing incidence spectrometer was designed to measure the diffuse extreme ultraviolet background. It was flown on a sounding rocket, and data were obtained on the diffuse background between 80 and 650 Å. These are the first spectral measurements of this background below 520 Å. Several emission features were detected, including interplanetary He I 584 Å emission and geocoronal He II 304 Å emission. Other features observed may originate in a hot ionized interstellar gas, but if this interpretation is correct, gas at several different temperatures is present. The strongest of these features is consistent with O V emission at 630 Å. This emission, when combined with upper limits for other lines, restricts the temperature of this component to $5.5 < \log T < 5.7$, in agreement with temperatures derived from O VI absorption studies. A power-law distribution of temperatures is consistent with this feature only if the power-law coefficient is negative, as is predicted for saturated evaporation of clouds in a hot medium. In this case, the O VI absorption data confine the filling factor of the emission to $f \leq 4\%$ and the pressure to more than 3.7×10^4 cm^{-3} K, substantially above ambient interstellar pressure. Such a pressure enhancement has been predicted for clouds undergoing saturated evaporation. Alternatively, if the O V emission covers a considerable fraction of the sky, it would be a major source of ionization. A feature centered at about 99 Å is well fitted by a cluster of Fe XVIII and Fe XIX lines from gas at $\log T = 6.6$–6.8. These results are consistent with previous soft X-ray observations with low-resolution detectors. A feature found near 178 Å is consistent with Fe X and Fe XI emission from gas at $\log T = 6$; this result is consistent with results from experiments employing broad-band soft X-ray detectors.

Subject headings: instruments — interstellar: matter — line identifications — ultraviolet: spectra — X-rays: spectra

1. INTRODUCTION

It has been more than 30 years since it was first suggested that hot, million-degree gas exists within our Galaxy (Spitzer 1956), and more than 20 years since the soft X-ray background was first detected (Bowyer, Field, & Mack 1968). It is now generally believed that this diffuse soft X-ray background is produced by a high-temperature component of the interstellar medium. However, evidence of the thermal nature of this emission is indirect in that it is based not on observations of line emission, but on the indirect evidence that no plausible nonthermal mechanism has been suggested which does not conflict with some component of the observational evidence.

The distribution of the soft X-ray background has been observed in detail with proportional counters that have limited energy resolution (McCammon et al. 1983; Marshall & Clark 1984). Measurements with greater resolution have been obtained with a gas scintillation proportional counter (Inoue et al. 1979). These results show an enhancement near 20 Å which has been suggested to be O VII emission from a 10^6 K plasma. Inoue et al. modeled their spectrum with emission from a 10^6 K isothermal plasma absorbed by intervening neutral material. The model has a strong O VII line along with other lines that blend together to fit an observed feature at 20 Å. The instrument's resolving power ($\lambda/\Delta\lambda$) is only about 2 at 44 Å and is not high enough to resolve the individual emission lines of this model.

Measurements of the soft X-ray spectrum have been made by Schnopper et al. (1982) and by Rocchia et al. (1984) with a lithium-drifted, silicon solid-state detector. This instrument has resolution similar to that of the gas scintillation proportional counter used by Inoue et al. (1979). In addition to detecting the 20 Å feature reported by Inoue et al., Rocchia et al. (1984) suggest that lines of C V and C VI at 40 Å were detected. Unfortunately, the instrument's long-wavelength cutoff is near 40 Å and consequently the data show only one side of this emission enhancement, and there is no indication that the intensity drops at wavelengths larger than 40 Å.

A minimal amount of data on the background in the extreme ultraviolet (EUV) has been obtained with broad-band detectors. The diffuse EUV background was first detected with a Berkeley sounding rocket experiment (Cash, Malina, & Stern 1976). These measurements covering the 115–155 Å band were later confirmed by the data obtained with the Apollo-Soyuz EUV telescope, which performed longer observations of different regions of the sky in the same band (Stern & Bowyer 1979). Bloch et al. (1986) used a sounding rocket experiment to scan a portion of the sky in the 115–155 Å band. These experiments are the only ones to have detected diffuse background radiation; all other observations have produced upper limits to the background intensity.

Stern and Bowyer found that the emission was consistent with the temperatures inferred from the soft X-ray measurements but that some gas must be at cooler temperatures, $T \lesssim 4 \times 10^5$. Bloch et al. (1986) found no evidence for cooler gas; their analysis is consistent with the temperature derived from the X-ray measurements.

In addition to the 115–155 Å band measurements with the Apollo-Soyuz EUV telescope, data were obtained on the diffuse background in bands covering 170–620 and 500–800 Å. Unfortunately, the intensity measured

[1] Current postal address: Space Sciences Laboratory, University of California, Berkeley, CA 94720.

[2] Also with the Astronomy Department, University of California, Berkeley.

dominated by the bright, resonantly scattered solar He II at 304 Å and He I at 584 Å, making direct observation of interstellar lines impossible. Stern and Bowyer analyzed the *Apollo-Soyuz* observations in the antisolar direction, where the scattered 304 Å geocoronal line intensity is greatly reduced, to obtain upper limits on the interstellar intensity. Paresce & Stern (1981) argued that the residual signal in this band is consistent with emission from a single line at 584 Å. They employed a differencing technique to obtain a more stringent upper limit on this intensity. While this approach may be valid, such a procedure adds considerable uncertainty to the result.

Holberg (1986) analyzed data from 1,508,198 s of observations at high Galactic latitude with the *Voyager 2* ultraviolet spectrometer. The EUV part of this observation is dominated by the solar He I 584 Å line intensity that is resonantly scattering from neutral helium flowing through the solar system. Holberg removed this bright He I line from his spectra along with other sources of background to derive upper limits to interstellar emission between 520 and 1100 Å.

If the diffuse EUV background is the product of emission from a hot gas, most of the radiated power will be concentrated in emission lines from highly ionized atoms (Kato 1976; Shapiro & Moore 1976; Raymond & Smith 1977; Stern, Wang, & Bowyer 1978; Mewe, Gronenschild & van den Oord 1985). Hence spectral measurements will not only provide definitive proof of the existence of a hot component of the ISM, but they will also provide useful diagnostics of this gas. Despite this compelling motivation, spectral measurements have not previously been made at EUV wavelengths shorter than 520 Å. The reason lies in the difficulty of building grazing incidence diffuse spectrometers.

In § 2 we describe our diffuse EUV spectrometer and our observations obtained on a sounding rocket flight. In § 3 we describe the tests performed on the data to search for emission lines. In § 4 we provide an interpretation of the observation with respect to emission from hot interstellar gas. The implications of our findings are discussed in § 5, and a summary of our results is provided in § 6.

2. INSTRUMENTATION AND FLIGHT

The spectrometer described here was designed specifically to observe the EUV background radiation. The instrument is an objective grating, grazing incidence spectrometer. A wire grid collimator restricts the field of view in one dimension to 40', while allowing 15° of sky to enter the instrument in the orthogonal direction. This wedge of light is diffracted by an array of flat, blazed reflection gratings at grazing incidence. Once diffracted, the light is focused in the spectral direction by an array of mirrors through thin film bandpass filters and onto microchannel plate detectors. A schematic of the spectrometer is shown in Figure 1.

The total instrument payload consists of three such spectrometers, each tailored to a specific wavelength range. To obtain higher sensitivity at shorter wavelengths, the spectrometer that covers 80–230 Å has 44 cm² of collecting area, about twice the area of each of the other two spectrometers. The medium-wavelength spectrometer covers 230–430 Å, and the long-wavelength spectrometer covers 430–650 Å. The latter two spectrometers have higher resolution than the short-wavelength system because of the requirement that the bright He I and He II solar system lines be separated from the much weaker interstellar lines. The two longer wavelength spec-
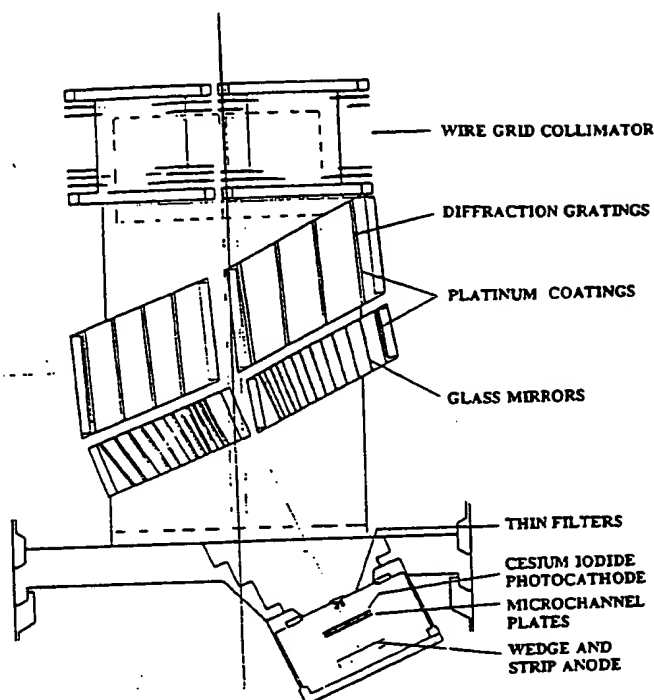

FIG. 1.—Schematic of the diffuse EUV spectrometer.

trometers both focus on different parts of the same imaging detector.

The grasp of the spectrometer, defined as the effective area integrated over the solid angle, is shown in Figure 2. Absolute detector efficiency and absolute effective area were measured relative to either an EUV diode calibrated by the National Bureau of Standards or to a proportional counter with known window transmission and gas efficiency. The spectrometer resolution, shown in Figure 3, was measured with narrow beams of EUV radiation entering the spectrometer at a variety of angles and positions across the instrument. Ray trace analysis of the system shows that the spectrometer resolution varies smoothly with wavelength; therefore, the estimated
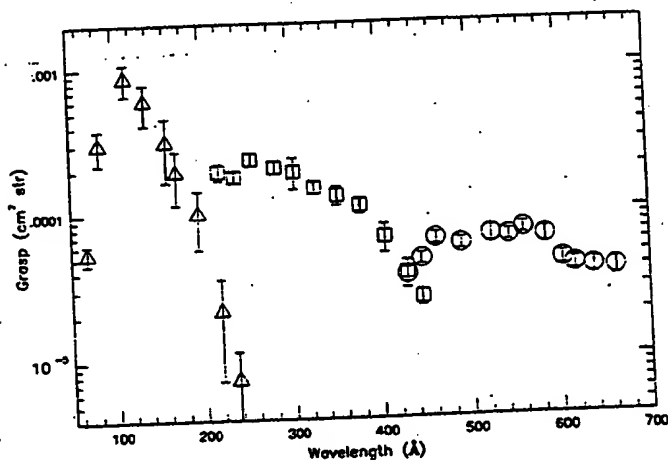

FIG. 2.—The spectrometer grasp (A_{eff} Ω) as a function of wavelength. The short-, medium-, and long-wavelength spectrometer measurements are indicated by the triangles, squares, and circles, respectively.
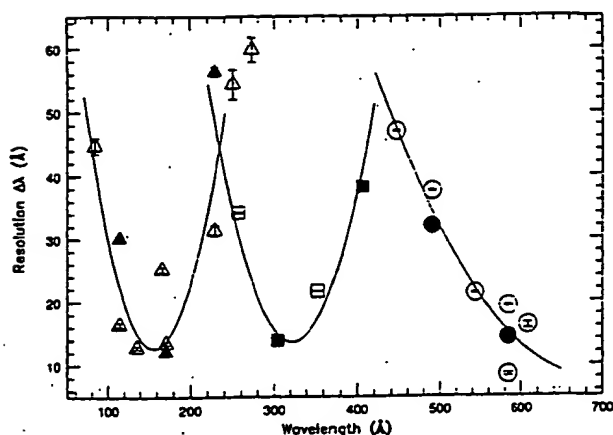
FIG. 3.—The resolution (FWHM in Å) as a function of wavelength. The triangles show the short-wavelength system resolution, and the squares and circles show the medium- and long-wavelength systems; respectively. The open symbols indicate measurements made prior to launch, and the solid symbols show postflight measurements. The error bars shown are the 80% confidence intervals to the fits of each measurement, and the curves are parabolae that have been fit to the data.

resolution measurements have been fit to parabolic curves, as shown in Figure 3. These curves are taken as a reasonable estimate of the instruments' resolution, and the scatter of the measurements about the curve as an indicator of the total uncertainty of the individual measurements.

The spectrometer was designed to avoid false line problems, and the assembled instrument was tested extensively to check for "ghost lines" and to determine the effects of scattered light and particle infiltration. Intense beams of 170 Å, 304 Å, 584 Å, and 1216 Å radiation, and electrons and ions with energies up to 400 eV were scanned across the instrument while aimed directly down the optical axis and at 5° and 10° to either side of the axis. Images accumulated during these tests show no signs of any ghost lines with count rates thousands of times higher than those observed in the brightest line (584 Å) during flight. The tests with low-energy particles and radiation outside a given spectrometer's bandpass showed no measurable increase in count rate over the detector background of that spectrometer. Furthermore, no increase in count rates were seen in any spectrometer when radiation of any wavelength was incident at angles outside the central 40' field of view of the collimator.

If filter pinholes developed before the observation, intense 1216 Å radiation scattering through the instrument could have entered the detector chamber. In this case, the scattered light would appear only as an increased detector background unless there were intrinsic detector nonuniformities that mimicked line emission. Therefore, many points on the detector surface were measured to test for fluctuations in quantum efficiency over different regions of the detector. These measurements showed the detector response to be quite uniform. The entire detector area was also illuminated with a diffuse beam of far-ultraviolet (FUV) radiation. These flat-field images have been examined for signs of line emission in the exact same manner as the flight data. No lines were found in this flat-field test data.

The diffuse EUV spectrometer was launched from White Sands, New Mexico, at 10 minutes after midnight (MST), 1986 April 22, on a Nike-boosted Black Brant sounding rocket. The rocket reached an apogee of 303.9 km at 283 s after launch. The spectrometer was pointed in the antisolar direction, down

Earth's shadow. This position was held for 160 s and then shifted 1°.5 along the narrow (40') field of view and held for another 160 s. As detailed later, this shift helped to determine the point source contribution to the observed emission. The flight ended with a scan away from Earth's shadow toward the southern horizon. The pointing was centered at the position $l = 325°.0 \pm 0°.5$, $b = 47°.7 \pm 0°.5$, as confirmed by a 35 mm star camera which photographed the sky every 5 s during the flight.

Postflight calibration of the instrument alignment and resolution and a partial throughput test were performed within 1 month of the launch. The alignment was within 4% of the preflight values, and the postflight resolution measurements indicated by the solid symbols in Figure 3, were all within 45% (2.3 σ) of their preflight values. Unfortunately the aperture door on the optics cavity lost its vacuum seal during recovery, causing a rupture of the thin filters and eliminating the possibility of carrying out a complete postflight throughput test. We did, however, measure the postflight throughput without filters, which we then corrected with the preflight measured filter transmissions. The result was consistent with the preflight measurement to better than 45% (1.2 σ). The spectrometer system is described further in Labov (1988a, b, 1989).

3. DATA ANALYSIS

A raw spectrum was derived for each spectrometer from photons detected while the instrument was pointed in the anti-solar direction and while the detectors were operating at constant background levels. The short-wavelength spectrum (80–230 Å) includes 329 s of data with a detector background level at 1.0 counts s^{-1} cm^{-2}. The medium- and long-wavelength spectra (230–650 Å) include 234 s of data with a detector background level of 1.6 counts s^{-1} cm^{-2}. The constant background of the detectors was about twice the background observed in the laboratory, which is common for these detectors at these altitudes. The resultant spectrum is shown in Figure 4. The width of the pixels in Figure 4 is the electronic sampling and the minimum spectrometer line width covers five to six of these electronic pixels. Solar radiation at 584 Å is scattered by neutral helium flowing through the solar system clearly present in this figure, and features near 100 Å

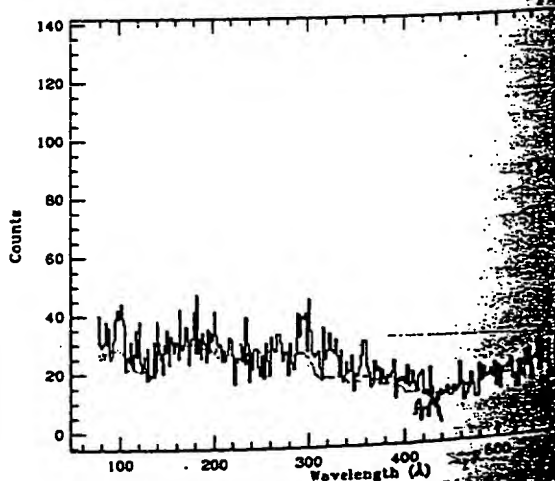

FIG. 4.—Raw spectra from all three spectrometers. The shows the number of counts accumulated in each wavelength antisolar pointing. The dotted line shows the detector back or smoothing has been performed.

610, and 635 Å are suggested. The dotted curve in Figure 4 indicates the overall shape of the detector background spectrum as measured in the laboratory, scaled by a factor of 2.

3.1. Tests for Emission Features

Since the signal to noise of our measurement was expected to be low, three criteria were established for a feature to be considered significant. First, the feature must not be due to a transient malfunction of the detector or spectrometer system. The postflight calibration (discussed in § 2) indicates that only the filters were damaged during the flight. The instrument has three independent vacuum pumps, each connected to one of the three chambers that are separated by the two filters. All these pumps were in operation after launch and prior to the observation. The pump voltage and current monitors showed that a pressure differential existed at this time, indicating that the filters were intact after the separation of the payload from the booster engines. At most, only a small pinhole could have been present during the observation. If such a filter pinhole did exist during the observation, or if a detector nonuniformity developed, the flight images would show a small region of enhanced count rate. However, since the spectrometers have no focusing perpendicular to the spectral direction, a true emission line will evenly illuminate the entire length of the detector. Several tests for uneven detector illumination were performed, and only one of the eight possible emission features detected was unevenly illuminated. That feature, located at 120 Å, was removed from subsequent analysis.

Second, the feature must not be a consequence of the method employed in establishing the continuum (or background) level. The detector background was established by summing the dark counts accumulated before and after the flight under a variety of conditions. An independent method of estimating the background continuum has also been applied. Detector images have been artificially created with perfectly uniform backgrounds in the active area of the detector. These "dummy" images are then processed in a manner identical to the flight data. This provides a relatively smooth continuum curve that includes the changes in background levels due to the change in image size as a function of wavelength. The analysis was carried out using both methods of continuum estimation; an emission line is a consequence of the noise in the background estimates, it will not appear in the analysis with the smooth dummy-image continuum. All the features discussed hereafter are present regardless of the method used to estimate the continuum.

Third, the feature must show a statistically significant rise above the continuum level. To find how many significant lines are in each spectrum, the raw spectrum was fitted with a model composed only of the continuum detector background spectrum multiplied by a scale factor. The model was fitted to the raw spectrum data by varying the continuum scale factor to minimize χ^2. A line was then added to the model at the wavelength corresponding to the largest residual in the fit with none. The wavelength and strength of this line, along with the continuum scale factor, were then varied to minimize χ^2. A second line was added at the wavelength corresponding to the largest residual in the fit with one line, and the wavelength and strengths of both lines were varied as well as the scale factor. This process was repeated with additional lines until no further improvement in the fit was noted. The wavelengths of the most probable lines were determined. Confidence intervals were determined for the strength

and wavelength of each line. Because of the low number of counts per bin in the raw spectra, the likelihood-ratio test described by Cash (1979) was used with the procedure described by Lampton, Margon, & Bowyer (1976) for determining confidence intervals. A similar technique was applied at all wavelengths across the spectra to determine upper limits to line radiation at each wavelength.

3.2. Tests for Noninterstellar Emission

Once an emission feature was established as being significant, all possible solar and stellar origins for this emission were considered. This section describes procedures designed to test different noninterstellar emission mechanisms that might, in principle, have contributed to the observed features.

The field of view in the target direction does not contain any of the FUV point sources listed in the TD-1 catalog (Jamar et al. 1976). This catalog includes all O- through B3-type stars brighter than seventh magnitude and other B stars to about sixth magnitude. With these sensitivity limits, the catalog includes all stars that are hotter than 12,000 K, have little interstellar extinction, and lie within the nearest 100 pc. Any FUV source likely to appear in the EUV is therefore included in this catalog. The diffuse EUV spectrometer field of view does not contain any of the X-ray sources in the HEAO A-2 catalog (Nugent et al. 1983) or the HEAO A-1 catalog (Wood et al. 1984). The A-2 catalog has a limiting sensitivity of 10^{-11} ergs cm^{-2} s^{-1} at 28–69 Å, and the A-1 catalog is complete to 250 μJy at 2.5 Å. If an uncataloged object with a flux equal to the limiting sensitivity of the HEAO surveys happened to be in the field of view of the spectrometer, that object would produce only a few counts at 100 Å during a 300 s observation by the diffuse EUV spectrometer.

The point source sensitivity of the diffuse EUV spectrometer is such that only the brightest known EUV sources (such as the hot white dwarf HZ 43) could produce a signal with count rates approaching those observed. No known white dwarfs hotter than 12,000 K are located near the field of view in the target direction (McCook & Sion 1984). Furthermore, white dwarfs are continuum emitters, not line emitters; therefore, if such an object were in the field of view, it could only raise the continuum level, not create lines. Similarly, only the brightest known EUV coronal emitters (such as α Cen) could be detected by the spectrometer. Halfway through the point observation, the instrument was shifted 1°5 in the narrow field of view direction. The flight data in each detected emission line were examined for changes corresponding to this shift. No change greater than 1 σ was observed in any of the lines or in the total count rate for any of the spectrometers. Since the probability of having two bright, unknown, and identical EUV sources separated by only 1°5 in a region that can extend ~100 pc is unlikely, we conclude that the emission observed is truly diffuse emission.

A possible noninterstellar source of diffuse EUV emission is resonantly scattered solar radiation. Since we observed in the antisolar direction down Earth's shadow cone, solar photons must be multiply scattered to reach the field of view of the spectrometer. If any of the detected features were geocoronal in origin, they would appear at least 40 times brighter in previous observations that were not confined to Earth's shadow (Weller & Meier 1974a; Chakrabarti et al. 1982). With the exception of He II 304 Å emission, radiation at these intensities is ruled out by the observations of Stern & Bowyer (1979) and Holberg (1986).

Another possible noninterstellar emission source is Earth's atmosphere. Spectra of the dayglow at wavelengths above 400 Å show several O II and N II emission lines, including an N II emission line at 629 Å (Chakrabarti et al. 1983). As atmospheric ions recombine at night, the intensity of the recombination lines will be significantly diminished. For example, the O I line at 989 Å is over 300 times brighter in the day than at night (Chakrabarti et al. 1983; Chakrabarti, Kimble, & Bowyer 1984). If the N II 629 Å dayglow emission is scaled down by this factor, it would be 25 times dimmer than the 635 Å feature reported here. Furthermore, several of the O II dayglow lines are much brighter than the N II 629 Å line, and none of these lines were found in the diffuse EUV spectrometer data. It therefore seems unlikely that the 635 Å feature is atmospheric in origin.

3.3. Line Strengths

The emission features that pass the criteria discussed in § 3.1 are summarized in Table 1. The wavelength and count rate of the line at 609 Å supports the hypothesis that it is 304 Å geocoronal He II emission detected in second order. Similarly, the feature at 200 Å is consistent with a second-order image of the 99 Å feature. The 200 and 609 Å intensities are therefore excluded from Table 1. The confidence intervals for the wavelengths are the single-side 1 σ confidence levels. These intervals include both the uncertainties in the fitting procedure and those associated with the wavelength calibration. The observed counts listed in column (2) are the total number of counts in the line after correction for background. The confidence levels here are those found in the fitting procedure. The statistical confidence listed for each line in column (5) includes an estimate of the systematic errors.

The intensities listed in Table 1 have been corrected for atmospheric absorption. This absorption was calculated with the cross sections of Kirby et al. (1979) combined with the MSIS-83 thermospheric composition model atmosphere (Hedin 1983). The atmospheric attenuation was calculated as a function of wavelength, altitude, and zenith angle and then averaged for the conditions encountered during the observation. The maximum average attenuation used was 10%. The confidence levels for the intensities included both statistical and instrumental calibration uncertainties. For convenience the intensities in Table 1 are listed in photons cm^{-2} s^{-1} sr^{-1} and in rayleighs (1 photon cm^{-2} s^{-1} sr^{-1} = $4\pi/10^6$ rayleighs).

The lines listed in Table 1 are presented in Figure 5 along with the upper limits to line emission. Also shown in Figure 5 is the strength necessary for a single line to produce the broadband upper limits from the Apollo-Soyuz EUV telescope obser-
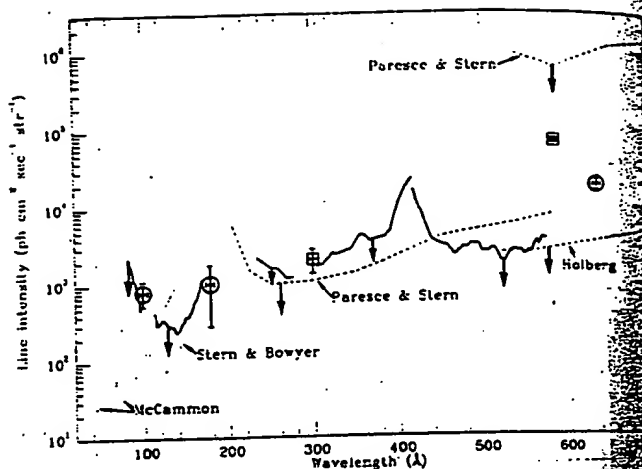

FIG. 5.—The emission features detected are indicated with 1 σ uncertainty in both wavelength and intensity. The uncertainties indicated include both calibration and fitting procedure uncertainties. The squares show the nonstellar lines (304 and 584 Å), and the circled points are the lines that are believed to be interstellar in origin. The bold lines indicate the upper limits (90% confidence level) to line radiation inferred from this observation. The dashed lines indicate the upper limits derived from previous observations; the dotted lines indicate the previous soft X-ray and EUV observations.

vations (Paresce & Stern 1981) and the upper to line radiation found with the Voyager instrument (Holberg 1986). In Figure 5 we show the single line strength that would produce the count rates observed in the soft X-ray carbon band (C band, Å), boron band (B band, 66–95 Å), and the beryllium band (Be band, 115–155 Å) (McCammon et al. 1983; Stern & Bowyer 1979).

As can be seen in Figure 5, the 178 Å line is consistent with the previous observations. Bloch et al. (1986) measured the B band intensity at two locations within 20° of the position observed. The 1 σ range in 178 Å intensity listed in Table 1 would produce between 2.5 and 17.7 counts s^{-1} in the proportional counter of Bloch et al. (1986). At $l = 355°$, $b = 43°$, Bloch et al. observed 7.2 ± 0.8 counts s^{-1}, and at $l = 351°$, $b = 41°$, 4.5 ± 0.6 counts s^{-1} were observed, both consistent with our measurement. Bloch (1988) has analyzed the height information from the Bloch et al. (1986) data and concludes that if the emission they observe is dominated by a single line, then that line must be below 135 Å. Due to the range in 178 Å intensities that are consistent with our data, we cannot confirm whether the Bloch et al. observations are dominated by emission at 178 Å or by emission at shorter wavelengths.

TABLE 1
OBSERVED EMISSION FEATURES

λ (Å)	OBSERVED COUNTS	INTENSITY		STATISTICAL CONFIDENCE
		photons cm^{-2} s^{-1} sr^{-1}	rayleighs	
$98.7^{+4.2}_{-5.3}$	191^{+40}_{-37}	790^{+270}_{-320}	$0.0100^{+0.0034}_{-0.0040}$	>0.99
$178.1^{+3.1}_{-2.6}$	57^{+33}_{-35}	1030^{+740}_{-780}	$0.013^{+0.009}_{-0.010}$	0.86
$200.4^{+3.3}_{-2.2}$	99^{+27}_{-44}	(Second order)	...	0.96
$299.7^{+3.9}_{-3.0}$	72^{+21}_{-23}	2080^{+720}_{-740}	$0.026^{+0.009}_{-0.009}$	0.99
$582.1^{+4.3}_{-4.3}$	738^{+32}_{-34}	$70,400^{+5600}_{-5700}$	$0.885^{+0.071}_{-0.072}$	>0.99
$609.1^{+4.9}_{-4.9}$	87^{+21}_{-16}	(Second order)	...	>0.99
$634.7^{+4.7}_{-4.7}$	113^{+17}_{-20}	$19,000^{+3000}_{-3500}$	$0.238^{+0.038}_{-0.044}$	>0.99

The 99 Å feature is within 2.2 σ of the B band intensity observed by McCammon et al. (1983). The 635 Å line plotted in Figure 5 is significantly above the upper limits of Holberg. If the emission is interstellar in origin, it would be subject to strong absorption by neutral interstellar hydrogen, and the brightness of the emission would be extremely sensitive to the geometry of the emitting and absorbing regions. Since our view direction was different from that of Holberg, our observations may not be in conflict.

4. INTERPRETATION

The feature observed at about 300 Å is the first spectroscopic detection of diffuse He II 304 Å geocoronal background, and the 609 Å feature is consistent with this 304 Å line observed in second order. The 304 Å intensity listed in Table 1 is consistent with the upper limit to 304 Å emission in the antisolar direction (0.02 rayleighs) reported by Paresce, Fahr, & Lay (1981). None of the other lines appear to emanate from Earth's geocorona. The 0.9 rayleigh 584 Å emission is consistent with solar radiation resonantly scattered by neutral helium flowing through the solar system; previous 584 Å measurements vary from 0.5 to 10 rayleighs (Weller & Meier 1974b; Freeman et al. 1976, 1977; Broadfoot & Kumar 1978; Weller & Meier 1979; Weller & Meier 1981; Dalaudier et al. 1984). This leaves three possible features, those at 99, 178, and 635 Å, which may be produced by the hot ISM. Calculations of the emission from a hot interstellar plasma show bright lines near these wavelengths produced by Si V, Ne VII, Ne VIII, Fe XVIII, or Fe XIX (99 Å); O VI or Fe VIII to Fe XI (178 Å); and O V (635 Å) (Stern, Wang, & Bowyer 1978; Raymond & Smith 1984; Mewe, Gronenschild, & van den Oord 1985).

For an analysis of these features we consider the ISM to consist of an emitting component with no self-absorption and of a second component which is purely absorbing. For an optically thin isothermal gas in which the emitting material is homogeneous along the line of sight, the total emission from the emitting region is

$$I^{\circ}_{\lambda} = \frac{1}{4\pi} \frac{\lambda}{hc} \frac{P_{\lambda}(T)}{n_e^2} \text{EM} , \qquad (1)$$

where EM is the emission measure, $P_{\lambda}(T)/n_e^2$ is the line power, and I°_{λ} is in photon units (photons cm^{-2} s^{-1} sr^{-1}).

The ISM models can be extended to include a distribution of temperatures; following Jenkins (1978b) and Paresce & Stern (1981), a power-law temperature distribution defined by

$$\frac{dn_e}{d \ln T} = C_e T^a \qquad (2)$$

is used. Here C_e is a scale factor that can be written in terms of filling factor and pressure of the ISM. This temperature distribution model is discussed in more detail by Paresce & Stern (1981) and Labov (1988b).

The observed line intensity I_{λ} can be calculated by multiplying the emitted line intensity I°_{λ} by the effective transmission of the ISM. The net absorption is affected not only by the amount of absorbing material in the line of sight, but also by the geometry of this material and how it is arranged relative to the emitting material. In the simple slab absorption model, the emitting material lies beyond the absorbing material, $I_{\lambda} = I^{\circ}_{\lambda} e^{-\sigma_{\lambda} N_H}$, where σ_{λ} is the photoelectric cross section hydrogen atom (Cruddace et al. 1974; Morrison & McCammon 1983). This model does not include the effects due

to clumping of the absorbing material; such effects were first examined by Bowyer & Field (1969) and later refined by Jakobsen & Kahn (1986). Jakobsen and Kahn's generalized "embedded clump" model describes the effect of a statistical distribution of absorbing clouds with a clumping factor η_{λ}^0 that is multiplied by the photoelectric cross section yielding the effective cross section: $\sigma_{\lambda \, \text{eff}} = \eta_{\lambda} \sigma_{\lambda}$. By using a power-law cloud distribution with an exponent of $\xi = -2$ and a maximum cloud size of $N_{H \, max} = 1.7 \times 10^{21}$ cm^{-2}, the clumping factor η_{λ} can be calculated at any wavelength as a function of the minimum cloud size $N_{H \, min}$ (Kahn & Jakobsen 1988; Labov 1988b). Jakobsen & Kahn (1986) also define a macrogeometrical parameter R as the ratio of scale heights of the absorbing gas to the emitting gas: $R = \beta_a/\beta_e$. By varying the two parameters, $N_{H \, min}$ and R, this model can encompass a large variety of geometries and clumping.

The most straightforward approach is to consider our line strengths and upper limits directly in terms of the models of the ISM discussed above. In practice this is possible with only one of the three features observed, the feature at 635 Å. At long wavelengths the higher resolving power of the spectrometer, coupled with the limited number of strong lines produced at these wavelengths, makes it possible to analyze this feature directly. The most likely origin of this feature is O V emission at 629.7 Å. Within the 3 σ confidence interval for the wavelength of this feature, the next strongest line produced by a cosmic composition of gas at temperatures between log $T = 5$ and 7 is more than two orders of magnitude weaker (Stern, Wang, & Bowyer 1978; Raymond & Smith 1984). Two of these other lines are N II lines, including one at 635 Å. This N II line, however, would be accompanied by the N II 533 Å line, which is 16 times stronger. Any absorbing material in the line of sight will attenuate the 635 Å line more than the 533 Å line, making the apparent line ratio even larger. This 533 Å line was not observed. Since the strength of the observed 635 Å feature is 10 times larger than the upper limit at 533 Å, the 635 Å feature cannot be N II. Other lines within 3 σ of the observed 635 Å feature include C III (622.1 Å) and O II (644.2 Å), which can both be ruled out in the same way as the N II line. Additional nearby lines include Mg X (625.3 Å), O V (627.3 Å), N V (628.9 Å), and O VIII (632.7 Å). These are unlikely candidates because the emission measures and temperatures required to produce these lines would also produce bright lines at shorter wavelengths. Such lines were not observed. Another possible source of the observed feature at 635 Å is the [He I] $2\,^3S \rightarrow 1\,^1S$ line at 625.6 Å. This line is 2 σ from the recorded 635 Å feature, whereas the O V line is within 1 σ of the recorded feature. Therefore, in the following analysis it has been assumed that the feature at 635 Å is the 630 Å O V line.

Our observation places strong constraints on the temperature of the O V emitting gas. The O V 630 Å line is strongest at temperatures of $10^{5.4}$ K. An O IV line at 554 Å can be almost as strong as the O V 630 Å line at its peak emission temperature of $10^{5.3}$ K. This line was not detected. The ratio of the upper limit at 554 Å to the detected O V 630 Å emission is $I_{554}/I_{630} \cong 0.1$. This ratio places a lower limit on the temperature of log $T \geq 5.4$. A Ne VII line exists at 465 Å that peaks near log $T = 5.8$. This Ne VII line also was not detected, and the ratio of the upper limit at 465 Å to the detected 630 Å line strength is again about 1/10. This places an upper limit on the temperature of log $T \leq 5.7$. Absorption, in any geometry, will have a greater effect at 630 Å than at 465 or 554 Å and, therefore, further tightens these temperature constraints.
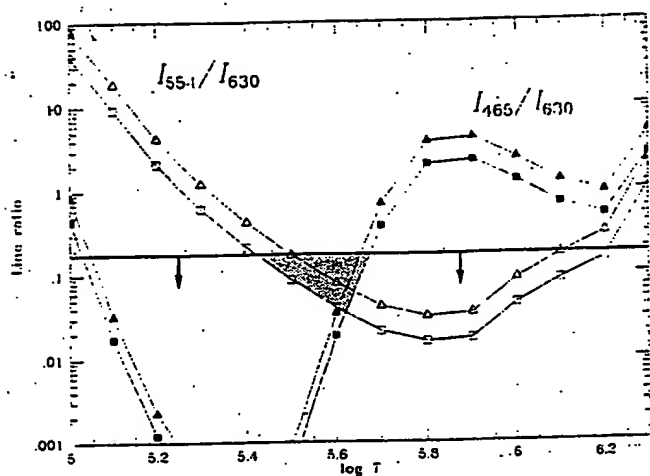
FIG. 6.—The ratio of the O IV 554 Å line to the O V 630 Å line as a function of temperature is shown by open symbols. The solid symbols indicate the Ne VII 465 Å to O V 630 Å line ratios. The predicted line ratios with no interstellar absorption are shown by the squares connected by solid lines, and the triangles show the line ratios predicted by a slab absorption model with a column density of $\log N_H = 18$. The solid horizontal line shows the upper limit imposed on both of these line ratios by the data reported here. The temperature of the emitting gas is restricted to the shaded region.

These results are shown in Figure 6. The line ratios with no absorption and with a slab absorption model where $\log N_H = 18$ are shown. We also show the 90% confidence upper limit for both lines which is provided by our results. The emitting material must produce line ratios which lie below this line and above the solid lines that show the case of emission with no absorption. This leaves only a small range of permitted temperatures: $5.42 \leq \log T \leq 5.67$. To test the sensitivity of these results to differences in plasma codes, the line ratios were calculated from both the code of Stern, Wang, & Bowyer (1978) and the code of Raymond & Smith (1984); the results were consistent to within 3%, showing that our conclusions are not particularly sensitive to differences in plasma codes.

The nonisothermal emission model defined in equation (2) has little effect on this temperature constraint. With a wide range of temperature exponents, $-2 < \alpha < 3$, the smallest I_{554}/I_{630} line ratio this model can produce is 0.4. Only by increasing the lower temperature limit $\log T_{min}$ to 5.5 can a line ratio as small as 0.1 be obtained. The I_{465}/I_{630} limit works with a full range of temperatures, $\log T_{min} = 5$ to $\log T_{max} \cong 7$, but the power-law coefficient α must be negative. These results are similar to the conclusion above; the I_{554}/I_{630} ratio is not consistent with a gas at temperatures less than $10^{5.5}$ K. The $\alpha < 0$ constraint from the I_{465}/I_{630} implies that the gas density decreases as the temperature increases. Therefore a higher temperature component, or a distribution of temperatures higher than $10^{5.5}$ K, could exist as long as the emission measure of the hotter material does not exceed the emission measure of the $\log T = 5.5$ gas. The hotter material in this gas can coexist with the $10^{5.5}$ K gas because the strongest lines at higher temperatures are only 1/10 as powerful as the O V 630 Å line at $10^{5.5}$ K.

These line ratio calculations utilized line power calculated under the assumption of ionization equilibrium. If the gas is cooling from a 10^6 K equilibrium state, the calculations of Shapiro & Moore (1976) show that the ions do not recombine quickly enough to remain in equilibrium, and so each stage of

ionization persists at lower temperatures. This does not, however, prevent recombination into O IV at about the same temperature ($10^{5.3}$ K). Similarly, the temperature of the Ne VII peak ($10^{5.78}$ K) is the same in the steady state and time-dependent calculations. Nonequilibrium ionization, therefore, does not effect the above conclusion that at least one component of the gas must be at a temperature near $10^{5.5}$ K.

The features centered at 99 and 178 Å, if produced by a hot ISM, will be produced by clusters of lines. The resolution of the spectrometer at these wavelengths is not high enough to identify any one emission line in these features. Hence it is necessary to generate model spectra and compare them with the spectra observed. To this end we generated synthetic spectra from isothermal models of the ISM with both slab and embedded clump geometries using line strengths from Raymond & Smith (1984) and interstellar absorption from Cruddace et al. (1974) and Morrison & McCammon (1983). The 90% and 99% confidence limits for emission measure and temperature for a slab absorption model with N_H as a free parameter are shown in Figure 7. In this model only values of $\log N_H$ less than 21.5 can fit the data. The results from the embedded clump model with $N_{H\,min}$ and R as free parameters are also shown in Figure 7. Both the slab absorption and the embedded clump isothermal models are dominated by the $\log T = 5.5$ solution. Since the embedded clump model includes a large range of absorbing geometries, it is consistent with a large range of emission measures. To determine values of $N_{H\,min}$ and R, at least two lines originating from the same gas are necessary. Since only one of the features observed with the diffuse EUV spectrometer originates at $\log T = 5.5$, these data cannot substantially constrain the $N_{H\,min}$ and R parameters, and only solutions with $\log N_{H\,min} < 18$ can be rejected. This restriction corresponds to rejection of any solution with a relatively smooth unclumped absorbing medium.

The results shown in Figure 7 confirm our results discussed above for the O V 630 Å emission feature. However, an isothermal model with $\log T = 5.5$ produces no emission at 99 or 178 Å. To reproduce the observed 99 and 178 Å features
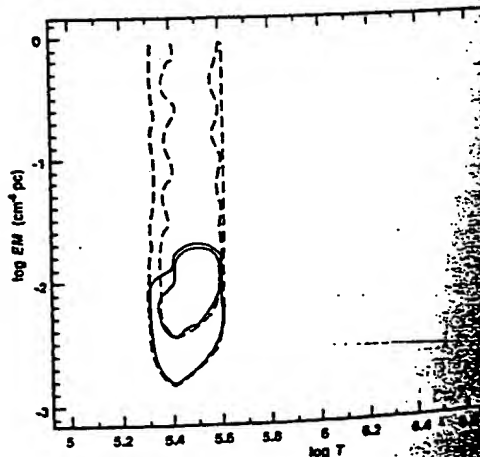

FIG. 7.—Results from fitting isothermal emission models reported here. The solid contours show the 90% and 99% for the slab absorption model including columns of $\log N_H = $ and 21. The dashed contours show the 90% and 99% for the fits to the embedded absorber model. In this model $\log N_{H\,min} = 17, 18, 19, 20,$ and 21 are included, with $R = 1$ and 10.

model with more than one temperature is required. A multiple temperature slab absorption model with N_H a free parameter, one temperature fixed at log $T = 5.5$, and the Wisconsin B and C band intensities (McCammon et al. 1983) included as upper limits provided an improved fit to the data. This model required a total of three temperatures to reproduce the observed features. In addition to the log $T = 5.5$ component, a solution near log $T = 6.8$ and log EM $= -1.8$ produces several Fe XVII and Fe XIX lines near 99 Å. The other solution near log $T = 6.0$ and log EM $= -2.0$ produces no lines near 99 Å, but it does produce a cluster of Fe X and Fe XI lines near 178 Å. Synthetic spectra were also generated with the plasma emission code of Mewe, Gronenschild, & van den Oord (1985) below 300 Å, and the code of Stern, Wang, & Bowyer (1978) above 300 Å. The model-fitting results were always similar to the results described above which were obtained with the Raymond & Smith (1984) code.

5. DISCUSSION

5.1. The 635 Å Line

The 635 Å line is consistent with emission from O V at 630 Å originating in gas at log $T = 5.5$. This gas will not produce emission lines at 99 or 178 Å, nor will it produce the observed soft X-ray intensity. This implies that hot gas exists at log $T = 5.5$, in addition to the gas emitting soft X-rays. In this section we examine other evidence for interstellar gas at log $T = 5.5$ and the implications of the O V emission for the ISM.

We first compare the temperature constraints provided by our observation with temperature constraints from O VI absorption studies. The star α Vir (Spica) is 6°6 away from the position we observed. This spectroscopic binary is at a distance of 84 ± 25 pc, has a hydrogen column of $N_H = 1.0 \pm 0.25 \times 10^{19}$ cm^{-2}, and an O IV column of $N_{O VI} = 2.69 \times 10^{13}$ cm^{-2} (York 1974; Jenkins 1978a; Bohlin, Savage, & Drake 1978; Paresce 1984). The average density of the O VI column to α Vir is 3.7 times the global average (Jenkins 1978b).

Absorption from N V was not observed along the line of sight to α Vir (York 1974). The upper limit to the N V/O VI ratio constrains the temperature to $5.53 \le \log T \le 5.75$. York analyzed the line widths to make an independent estimate of the upper temperature limit of the absorbing O VI gas. In the direction of α Vir, he finds log $T < 5.6$. The temperature constraints imposed by our observation of O V emission at 630 Å are nearly identical to the constraints obtained by York and are explainable by the presence of gas near $10^{5.5}$ K that absorbs O VI radiation and emits O V line radiation. We next consider the strength of the 635 Å line and the implications of the inferred emission measure. We use the relationship

$$\text{EM} = \int n_e^2 \, ds = f L n_e^2 = f L \left(\frac{p/k}{1.91T}\right)^2 , \quad (3)$$

where L is the path length, f is the filling factor of the hot gas, p is the pressure. Since the total galactic N_H observed in the direction of α Vir corresponds to an attenuation of 10^{10} at 630 Å, the distance to α Vir, 84 pc, is a good upper limit to L. Setting log $T = 5.5$ and log EM ≥ -2.5 from our results and $L = 84$ pc, equation (3) limits the pressure to $p/k \ge 3.7 \times 10^3 f^{-1/2}$ cm^{-3} K. This is consistent with measured thermal pressures in diffuse clouds (Jenkins, Jura, & Loewenstein 1983) and the pressure inferred from broad-band soft

X-ray measurements (Shapiro & Field 1976; Cox & Snowden 1986; Snowden et al. 1990).

The filling factor can be constrained if one assumes that the gas observed in absorption toward α Vir is typical of what we observed in emission. With this assumption, the O VI column density observed toward α Vir can be combined with our O V emission measure to estimate directly the filling factor and pressure. The electron density in the O VI absorption regions can be estimated by

$$n_e = n_{O VI}\left[\frac{O}{O VI}\right]\left[\frac{H}{O}\right]\left[\frac{e}{H}\right]. \quad (4)$$

At log $T = 5.5$, the O VI/O ratio is 25% in steady state ionization equilibrium (Raymond & Smith 1984; Shapiro & Moore 1976). With the abundances of Allen (1973), equation (4) reduces to $n_e = 7.12 \times 10^3 n_{O VI}$. The O VI density is related to the average O VI density by the filling factor $f: n_{O VI} = \langle n_{O VI} \rangle f^{-1}$. Combining this relation with equations (3) and (4) gives $p/k = 2.68 \times 10^{-4} T$ EM $L^{-1} \langle n_{O VI} \rangle^{-1}$ and $f = 5.07 \times 10^7 L \langle n_{O VI} \rangle^2$ EM^{-1}. Inserting the lower limit to the observed emission measure and the upper limit to the length of the emission region ($L \le 84$ pc), we find $p/k \ge 3.0 \times 10^4$ cm^{-3} K and $f \le 1.5\%$. This pressure is larger than the predicted thermal pressure of the local hot gas.

If the gas were not in a steady state situation but had been heated to log $T = 6$ and is now cooling through log $T = 5.5$, the ionization balance would be shifted, leaving less gas in both the O V and O VI ionization stages (Shapiro & Moore 1976). However, time-dependent ionization does not change the difference between the emission measure predicted from O VI absorption and the emission measure observed for O V emission, and hence our results would not be altered.

If the observed 630 Å O V emission originates from a nonisothermal gas, an analysis similar to that above can constrain the pressure and filling factor of the emitting region. In § 4 we showed that a power-law temperature distribution (equation (2)) can exist only if the minimum temperature of the gas is $10^{5.5}$ K and the exponent of the distribution is negative. Such a distribution is not consistent with classical evaporating clouds as described by McKee & Cowie (1977). If the cloud evaporation is saturated, however, a negative exponent of $\alpha = -5/4$ describes the temperature distribution in the saturated zone (McKee & Cowie 1977; Cowie & McKee 1977). If the lower temperature can be held at log $T = 5.5$, and if the region is saturated, it is possible that the observed emission originates in a dense interface. With $\alpha = -5/4$, log $T_1 = 5.5$, and log $T_2 = 6.0$, the pressure in the nonisothermal gas is $p/k = 1.23 \times 10^3 T_1^{1/2} L^{-1/2} f^{-1/2}$ cm^{-3} K, where L is in parsecs. The lower limit emission measure that is compatible with the data, log EM ≥ -2.5, corresponds to a minimum line intensity of 3.0×10^3 photons cm^{-2} s^{-1} sr^{-1}, restricting the pressure to $p/k \ge 7.4 \times 10^3 f^{-1/2}$ cm^{-3} K.

As with the isothermal case, the O VI absorption data for α Vir can be used to restrict the filling factor and the pressure independently. Combining equations (2) and (4) yields the average O VI density expected from a given temperature distribution. Using the steady state ionization fractions from Shapiro & Moore (1976) with the maximum emission length and minimum intensity derived from our observation, the filling factor and pressure are found to be restricted to $f \le 4.0\%$ and $p/k \ge 3.7 \times 10^4$. In this case, however, a pressure above the ambient ISM pressure is expected. For highly satu-

rated evaporation, Cowie & McKee (1977) find a relationship for this enhancement. For the values considered here, a pressure enhancement of 3.7 would be expected for a cloud size just under one parsec.

Regardless of the origin, the 635 Å emission observed could be a major source of ionization. Reynolds (1983, 1984, 1985) has shown that diffuse Hα emission is ubiquitous throughout the Galaxy, and widespread sources of flux shortward of 912 Å are required. Pulsar dispersion measures (Reynolds 1989) indicate a high scale height for the associated ionized material. Since the path length for radiation shortward of 912 Å is low, this implies that the ionizing source must also have a large scale height and be widespread. Transient heating appears unlikely, and the steady state ionization rate is more than can be provided by cosmic rays, the soft X-ray background, B stars, or hot white dwarfs (Reynolds 1986; Bruhweiler & Cheng 1988). Sciama (1990) and Salucci & Sciama (1990) have argued that a variety of observations can be explained by the presence of dark matter in the galaxy which decays with the emission of radiation below 912 Å.

The flux of 635 Å radiation required to produce hydrogen ionization is given by $F = \zeta_H/\sigma_\lambda = 4.3 \times 10^4 \zeta_{-13}$ photons cm^{-2} s^{-1}, where ζ_{-13} is the ionizing rate in units of 10^{-13} s^{-1} per H atom. Reynolds (1986) estimates that in the immediate vicinity of the Sun, a steady state ionizing rate of ζ_{-13} between 0.4 and 3.0 is required. To produce this range of ionization, the 635 Å intensity we observe would have to be distributed over 7%–54% of the sky.

5.2. The 99 and 178 Å Features

The 178 Å feature can be produced by a group of Fe X and XI lines at log $T = 6$. The best-fit emission measure for this gas is log EM = −2.0, implying a pressure of $p/k = 1.9 \times 10^4/\sqrt{fL_2}$ cm^{-3} K, where L_2 is the path length in units of 100 pc. With L_2 and f near 1, this pressure is only slightly above the overall pressure of the local ISM. Bloch (1988) finds that depleted abundances are required to fit an interstellar emission model to his Be band data. There is too much uncertainty in our 178 Å intensity to determine if the log $T = 6$ gas is depleted.

The 99 Å feature is best fitted by gas at log $T = 6.6$–6.8, where a complex of Fe XVIII and Fe XIX lines contribute. At the temperature of log $T = 6.6$–6.8, the bulk of the emission will be emitted in the 14–25 Å range (Raymond & Smith 1984; Mewe, Gronenschild, & van den Oord 1985). In the direction observed by the diffuse EUV spectrometer, the Wisconsin 13–28 Å M_1 band is 3 times brighter than the average high-latitude intensity, and the 11–20 Å M_2 band is about 2 times brighter than average (McCammon et al. 1983). At log $T = 6.6$–6.8, the emission measure required to produce the Wisconsin M_1 band count rate is log EM = −1.9 to −1.7 and the M_2 band count rate requires log EM = −2.3 to −2.1 (McCammon et al. 1983). These emission measures are in agreement with the lower limit of log EM ≥ −2 derived from the observations reported here.

In regions with similar M band enhancements, Inoue et al. (1980) reported a temperature of log $T = 6.5$, and Rocchia et al. (1984) found evidence for two temperatures, log $T = 6$ and log $T = 6.7$. The high-temperature component found by

Rocchia et al. (1984) has a 90% confidence interval of $6.63 \leq \log T \leq 6.72$ and an emission measure between log EM = −2.0 and −1.7, which is consistent with our results.

6. SUMMARY

We have designed and built a spectrometer to measure the diffuse EUV astronomical background radiation. Results from our sounding rocket observation reveal five emission-line features, two of which appear in first and second order. The strongest emission line is solar backscattered He I 584 Å radiation. Solar 304 Å radiation resonantly scattered by geocoronal He II was observed in both first and second order. Each of the three remaining spectral features is consistent with those expected from hot interstellar gas. Of these features, the strongest is the feature at 635 Å, which we tentatively identify as 630 Å O V emission. This emission, when combined with upper limits for other lines which were not observed, restricts the temperature of this gas to $5.5 < \log T < 5.7$, which is consistent with temperatures derived from O VI absorption studies. A power-law distribution of temperatures is consistent with the data only if the minimum temperature is $10^{5.5}$ K and the power law of the distribution is negative.

The isothermal models that best fit our O V results have low absorption (log $N_H < 17.5$) and emission measures of log EM = −2.5. If the O VI absorption data from the nearby star α Vir is taken as typical for the region observed, then a filling factor of less than 1.5% and a pressure of more than 3.0×10^4 cm^{-3} K would be required; such a pressure is considerably out of equilibrium with the interstellar environment. With a negative power-law temperature distribution such as that predicted for saturated evaporation of clouds in a hot medium (McKee & Cowie 1977), the α Vir O VI absorption data confine the filling factor of the emission to $f \leq 4.0\%$ and the pressure to more than 3.7×10^4 cm^{-3} K. Such a pressure enhancement has been predicted for clouds undergoing saturated evaporation. Alternatively, if the 635 Å emission covers a considerable fraction of the sky, it would be a major source of ionization.

The 99 Å feature is best fitted by a cluster of Fe XVIII and Fe XIX lines from gas at log $T = 6.6$–6.8. Gas at this temperature, however, is consistent with the 11–28 Å observations of McCammon et al. (1983), and it is compatible with results found by low-resolution spectral observations (Rocchia et al. 1984). The range of emission measures for our solution is consistent with these previous observations. The feature found at 178 Å is consistent with Fe X and Fe XI emission from gas at log $T = 6$, which is the same temperature derived from 44–77 Å soft X-ray background observations.

REFERENCES

Allen, C. W. 1973, Astrophysical Quantities, 3d ed. (London: Athlone)
Bloch, J. J. 1988, Ph.D. thesis, University of Wisconsin, Madison
Bloch, J. J., Jahoda, K., Juda, M., McCammon, D., Sanders, W. T., & Snowden, S. L. 1986, ApJ, 308, L59
Bohlin, R. C., Savage, B. D., & Drake, J. F. 1978, ApJ, 224, 132
Bowyer, C. S., & Field, G. B. 1969, Nature, 223, 573
Bowyer, S., Field, G., & Mack, J. 1968, 217, 32
Broadfoot, A. L., & Kumar, S. 1978, ApJ, 222, 1054

Bruhweiler, F. C., & Cheng, K. P. 1988, ApJ, 335, 188
Cash, W. 1979, ApJ, 228, 939
Cash, W., Malina, R., & Stern, R. 1976, ApJ, 204, L7
Chakrabarti, S., Kimble, R., & Bowyer, S. 1984, J. Geophys. Res., 89, 5660
Chakrabarti, S., Paresce, F., Bowyer, S., Chiu, Y., & Aiken, A. 1982, Geophys. Res. Letters, 9, 2
Chakrabarti, S., Paresce, F., Bowyer, S., Kimble, R., & Kumar, S. 1983, J. Geophys. Res., 88, 4898
Cowie, L. L., & McKee, C. F. 1977, ApJ, 211, 135
Cox, D. P., & Snowden, S. L. 1986, Adv. Space Res., 6, 97
Cruddace, R., Paresce, F., Bowyer, S., & Lampton, M. 1974, ApJ, 187, 497
Dalaudier, F., Bertaux, J. L., Kurt, V. G., & Mironova, E. N. 1984, A&A, 134, 171
Freeman, J., Paresce, F., Bowyer, S., & Lampton, M. 1976, ApJ, 208, 747
Freeman, J., Paresce, F., Bowyer, S., Lampton, M., Stern, R., & Margon, B. 1977, ApJ, 215, L83
Hedin, A. E. 1983, J. Geophys. Res., 88, 10170
Holberg, J. B. 1986, ApJ, 311, 969
Inoue, H., Koyama, K., Matsuoka, M., Ohashi, T., & Tanaka, Y. 1979, ApJ, 227, L85
Inoue, H., Koyama, K., Matsuoka, M., Ohashi, T., Tanaka, Y., & Tsunemi, H. 1980, ApJ, 238, 886
Jakobsen, P., & Kahn, S. 1986, ApJ, 309, 682
Jamar, C., Macau-Hercot, D., Monfils, A., Thompson, G. I., Houziaux, L., & Wilson, R. 1976, Ultraviolet Bright-Star Spectrophotometric Catalogue (Paris: European Space Agency)
Jenkins, E. B. 1978a, ApJ, 219, 845
———. 1978b, ApJ, 220, 107
Jenkins, E. B., Jura, M., & Loewenstein, M. 1983, ApJ, 270, 88
Kahn, S., & Jakobsen, P. 1988, ApJ, 329, 406
Kato, T. 1976, ApJ, 30, 397
Kirby, K., Constantinides, E. R., Babeu, S., Oppenheimer, M., & Victor, G. A. 1979, Atomic Data Nucl. Data Tables, 23, 63
Labov, S. E. 1988a, Appl. Optics, 27, 1465
———. 1988b, Ph.D. thesis, University of California, Berkeley
———. 1989, Appl. Optics, 28, 5073
Lampton, M., Margon, B., & Bowyer, S. 1976, ApJ, 208, 177
Marshall, F. J., & Clark, G. W. 1984, ApJ, 287, 633

McCammon, D., Burrows, D. N., Sanders, W. T., & Kraushaar, W. L. 1983, ApJ, 269, 107
McCook, G. P., & Sion, E. M. 1984, A Catalogue of Spectroscopically Identified White Dwarfs, 2d ed. (Villanova, PA: Villanova Press)
McKee, C. F., & Cowie, L. L. 1977, ApJ, 215, 213
Mewe, R., Gronenschild, E. H. B. M., & van den Oord, G. H. J. 1985, A&AS, 62, 197
Morrison, R., & McCammon, D. 1983, ApJ, 270, 119
Nugent, J. J., et al. 1983, ApJS, 51, 1
Paresce, F. 1984, AJ, 89, 1022
Paresce, F., Fahr, H., & Lay, G. 1981, J. Geophys. Res., 86, A12
Paresce, F., & Stern, R. 1981, ApJ, 247, 89
Raymond, J. C., & Smith, B. W. 1977, ApJS, 35, 419
———. 1984, private communication, update to Raymond & Smith 1977
Reynolds, R. J. 1983, ApJ, 268, 698
———. 1984, ApJ, 282, 191
———. 1985, in Gaseous Halo of Galaxies, ed. J. N. Bregman & F. J. Lockman (Green Bank: NRAO), 53
———. 1986, AJ, 92, 653
———. 1989, ApJ, 339, L29
Rocchia, R., Arnaud, M., Blondel, C., Cheron, C., Christy, J. C., Rothenflug, R., Schnopper, H. W., & Delvaille, J. P. 1984, A&A, 130, 53
Salucci, P., & Sciama, D. W. 1990, preprint
Schnopper, H. W., et al. 1982, ApJ, 253, 131
Sciama, D. W. 1990, preprint
Shapiro, P. R., & Field, G. F. 1976, ApJ, 205, 762
Shapiro, P. R., & Moore, R. T. 1976, ApJ, 207, 460
Snowden, S. L., Cox, D. P., McCammon, D., & Sanders, W. T. 1990, ApJ, 354, 211
Spitzer, L., Jr. 1956, ApJ, 124, 20
Stern, R., & Bowyer, S. 1979, ApJ, 230, 755
Stern, R., Wang, E., & Bowyer, S. 1978, ApJS, 37, 195
Weller, C. S., & Meier, R. R. 1974a, J. Geophys. Res., 79, 1572
———. 1974b, ApJ, 193, 471
———. 1979, ApJ, 227, 816
———. 1981, ApJ, 246, 386
Wood, K. S., et al. 1984, ApJS, 56, 507
York, D. G. 1974, ApJ, 193, L127